Seismic and hydroacoustic effects of the May 29, 2010 submarine South Sarigan volcanic explosion: Energy release and interpretation

Jacques Talandier, Olivier Hyvernaud, Hélène Hébert, René C. Maury, Sébastien Allgeyer

Seismic and hydroacoustic effects of the May 29, 2010 submarine South Sarigan volcanic explosion: Energy release and interpretation.

Jacques Talandier[a,*], Olivier Hyvernaud[b], Hélène Hébert[a], René C. Maury[c], Sébastien Allgeyer[a]

[a] *Laboratoire de Détection et Géophysique, Département Analyse et Surveillance de l'Environnement, Commissariat à l'Energie Atomique et aux Energies Alternatives, Bruyères-le-Châtel, 91297 Arpajon, France*
[b] *Laboratoire de Géophysique, Commissariat à l'Energie Atomique et aux Energies Alternatives, BP 640 F-98713 Papeete, Tahiti, French Polynesia*
[c] *Université de Brest, CNRS, UMR 6538 Géosciences Océan, Institut Universitaire Européen de la Mer (IUEM), Place Nicolas Copernic, 29280 Plouzané, France*

* Corresponding author. Tel.: +33 557410768. *E-mail address*: jac.talandier@wanadoo.fr

ABSTRACT

The May 2010 submarine volcanic crisis of the shallow South Sarigan Seamount (Marianas arc) ended on May 29 by a violent explosion that emitted a 12 km high atmospheric plume and created a crater 350 m in diameter. The application of the multiphase localization method to the *Pg, P, T* phases of this explosion allows us to refine considerably (mainly based on the intense and impulsive *T* phases) the location of their source, that fits the position of the newly-formed South Sarigan crater. We highlight the numerous similarities of this final explosion with artificial underwater explosions (conventional or nuclear tests of known energy). Especially, the explosive nature of the source in the volcanic basement is confirmed by the similarity of the *P* phases with those of underground nuclear tests and the application of discriminating criteria Ms – mb. The explosive nature of the source in the water is also confirmedby the application of the identification criteria for hydroacoustic sources and the *T* phases exceptionally impulsive and of short durations. These similarities allow us to provide a rough evaluation of the energy released by the South Sarigan final explosion using the methods commonly applied to man-generated explosions. We estimate a minimal released energy of 1 kt (4.2 x 10^{12} J) for the seismic effects of the shock and ca 1 t of equivalent TNT (i.e. 4.2 x 10^{9} J) for the hydroacoustic effects of the explosive source in the water. The processes leading to this final explosion are discussed on the basis of the sequence of the earlier seismic and eruptive events. Within the Comprehensive Nuclear-Test Ban Treaty framework, this explosion that affected concomitantly the solid, liquid and subaerial media is the first well documented one having generated intense waves: (*P*), hydroacoustic (*T*), acoustic (infrasounds) and tsunamis.

Key words:
Submarine explosion, seismic and hydroacoustic effects, hydroacoustic discrimination, released energy, South Sarigan Seamount, Marianas arc.

1. Introduction

Nuclear or chemical explosions have been extensively used to establish relationships between the energy of the charge and the characteristics of the direct arrival of generated signals. Cole (1960) and

Willis (1963) have shown that the spectral properties of hydroacoustic signals recorded even at long distances can be traced back to the energy of the explosive source. Weston (1960) measured differences between the acoustic source levels of various size charges, while Chapman (1988) studied specifically the effects of small shallow explosives charges using data recorded in far field. The amplitude of the seismic *P* phases is also related to the energy of an explosion, and nuclear experiments have been used to establish relationships between the mb magnitude and the nuclear yield (Marchal et al., 1979; Bache, 1982), after adjustment of site effects. The ratio of magnitude mb / Ms has also been used effectively as a discriminator between explosions and earthquakes (Liebermann and Pomeroy, 1969; Murphy and Mueller, 1971; Aki et al., 1974; Murphy and Baker, 2001). Although natural explosions, usually of volcanic origin, are often very complex, some authors tried to determine their energy (Newhall and Self 1982; Weston 1960; Prejean and Brodsky, 2011; Mason et al., 2004; Crosweller et al., 2012). The May 2010 final explosion of South Sarigan submarine volcano is particularly interesting because it has been recorded in various physical domains, a feature which allows us to compare the different methods of energy estimation, and to study the physical coupling of the source.

Submarine explosive volcanism is less common and much less well understood than its subsubaerial equivalent (Zimanowski and Butter, 2003; Rubin et al., 2012). Direct observation during ca 13 hours using Remotely Operated Vehicles (ROVs) associated with hydrophone data was carried out at NW Rota-1 volcano, Marianas Arc (location shown in Fig. 1; Chadwick et al., 2008). Usually, submarine volcanic explosions are detected from their seismic (Talandier, 2004), hydroacoustic (Talandier and Okal, 1987; Dziack and Fox, 2002, Reymond et al. 2003; Talandier and Okal, 2016; Caplan-Auerbach et al., 2017; Tepp et al., 2019) and infrasonic effects (Whitaker, 1995), sometimes coupled with surface observations: discoloration of the sea (Yamamoto et al., 1991), emission of hydromagmatic plumes (Waythomas et al., 2010; Prejean and Brodsky, 2011), floating pumices (Paris et al., 2012). The May 2010 underwater eruption of the South Sarigan volcano in the Northern Mariana arc (Snellen et al., 2011; Green et al., 2013; Searcy, 2013; Embley et al., 2014) was similar in many respects to those of the other Mariana arc submarine volcanoes, although it occurred at a small volcanic edifice that was not considered active before this event.

Located ca 150 km north of Saipan in the Marianas arc (Fig. 1), between the small islands of Sarigan and Anatahan, South Sarigan was a poorly surveyed seamount thought to be inactive until it erupted in May 2010. Embley et al. (2007) described the regional tectonic context of this subduction zone, and the main bathymetric features of the area were mapped in 2002 and 2003 (Embley et al., 2014). South Sarigan seamount is part of a volcanic complex made of numerous andesitic cone edifices (Bloomer et al., 1989; Stern and Smoot, 1998), and its pre-eruption summit was located at depth of ca 200-350 m below sea level. No hydrothermal activity was observed in this area (Baker et al., 2008). The 2010 eruptive crisis started by small volcano-tectonic earthquakes on April 2, 2010 (Searcy, 2013). Their number increased until May 27, when broad-spectrum hydroacoustic events were first recorded. These events occurred more and more frequently during May 28. Figure 3 shows a histogram of the crisis based

on *T* phases recorded by the network of hydrophones of the International Monitoring System (IMS) located north of Wake Island (H11N1).

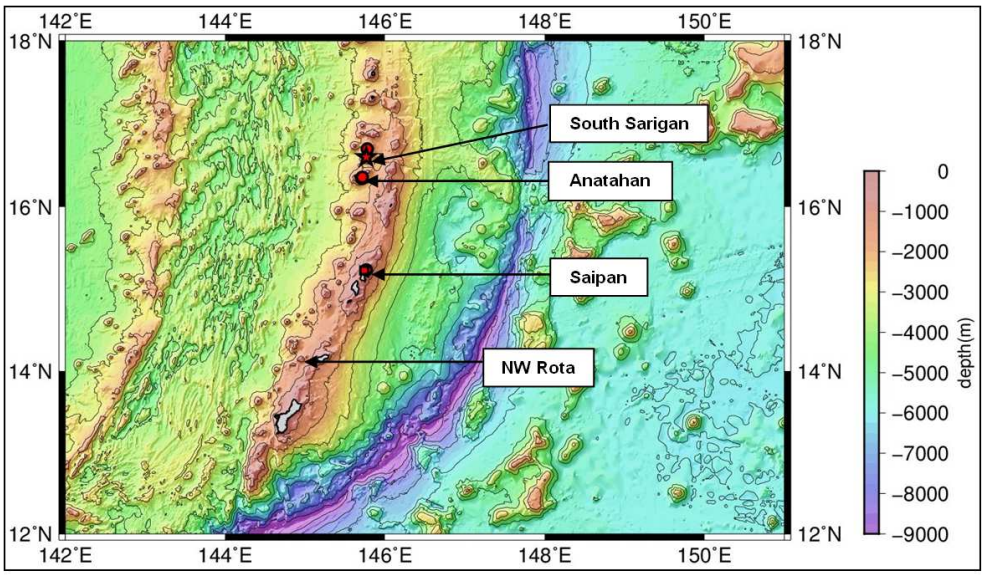

Figure 1: Bathymetric features of the Mariana Arc showing the location of South Sarigan, Saipan, Anatahan and Rota volcanoes. The bathymetry is from ETOPO-2 model (Smith and Sandwell, 1997). Contour interval 1,000 m.

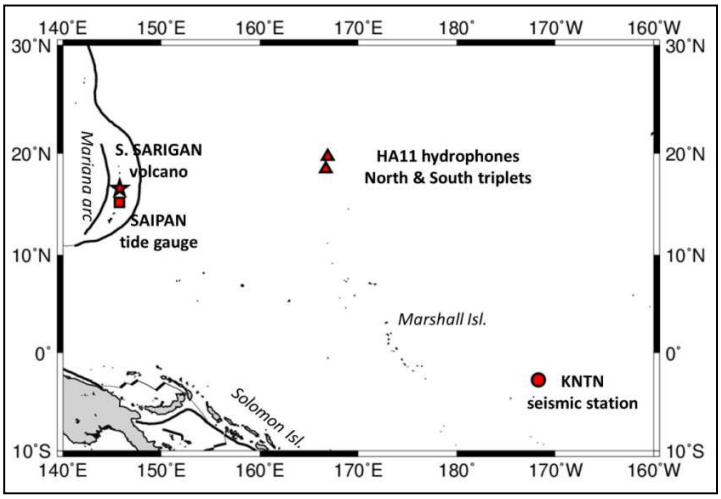

Figure 2: Map showing the locations of South Sarigan volcano and of the receiving stations including those of the International Monitoring System (IMS) network.

From May 28 to May 29 brief and impulsive events marked the propagation of cracks during magma ascent towards the surface (Figure 4 a). On May 29, between 3 and 8 hours UTC, tremors were directly generated by the underwater explosive magmatic expansion (Figure 4 b). This activity was mainly related to an underwater eruptive process often observed in the Mariana archipelago (Dziak et al., 2005; Chadwick et al., 2006; Embley et al. 2014; Tepp et al., 2019). Such common events related to magma ascent and expansion are also documented in Hawaii (Aki and Koyanagi, 1981; Chouet, 1981), the Tahiti-Mehetia Polynesian hot spot (Talandier and Okal, 1984; Talandier, 2004) and many other places. As

discussed by Chouet (1992), the fluid-filled crack model can explain the radiation of resonant seismic waves, with the resonance frequency and harmonic spacing being a complex function of the geometry of the cavity and of the mechanical properties of the two mediums (inside and outside the crack) controlled by the stiffness of the crack and the impedance contrast at the crack boundary. On the basis of video observations associated with hydrophones, Chadwick et al. (2008) analysed and interpreted the underwater explosive eruptions of volcano NW Rota-1 of the Mariana arc. The eruptive bursts recorded by a hydrophone located 100 m away from this volcano were similar to the tremors, shown in figure 4b, of a sequence recorded by the Wake Island far-field hydrophone H11N1. In both cases, many shaking sequences lasting 2 to 3 minutes and characteristic of explosive underwater magmatic activity were observed. In short, the initial phases of the South Sarigan eruption were similar to the crises previously described for the submarine volcanoes of the Marianas archipelago (Bloomer et al., 1989; Dziak et al. 2005*;* Chadwick et al., 2008; Anderson et al., 2017) until a paroxysmal explosion occurred several hours after the end of eruptive activity (Fig. 3). A plume of steam, gas and ash, that reached a probable height of 12 km according to the United States Geological Survey (USGS), rose above the site (Green et al., 2013). This violent isolated explosion was thus not the precursor of a more or less paroxysmal magmatic activity but the final event, delayed by 3h30 with respect to the end of the *T* phase sequences, ending the eruptive process. Post-eruption bathymetric surveys revealed that it produced a 350 m diameter breached crater with a broad apron downslope (Embley et al., 2014). Fresh andesitic lava blocks and pumices were recovered by ROV dives in the crater wall and the downslope deposits (Embley et al., 2014).

Although the seismic, hydroacoustic and acoustic (infrasonic) effects of the South Sarigan 2010 crisis have been thoroughly investigated (Green et al., 2013; Searcy, 2013), the numerous similarities of the violent explosion that ended it with artificial underwater explosions (conventional or nuclear tests) have not been highlighted. The aim of the present paper is to document these similarities, and to show that they enable a rough evaluation of the energy released by the South Sarigan explosion using methods commonly applied to man-generated explosions. In addition, this event, exceptional because of its energy and range of mediums (solid, liquid and subaerial) simultaneously involved allows us to test the main criteria of detection and identification of oceanic explosive sources.

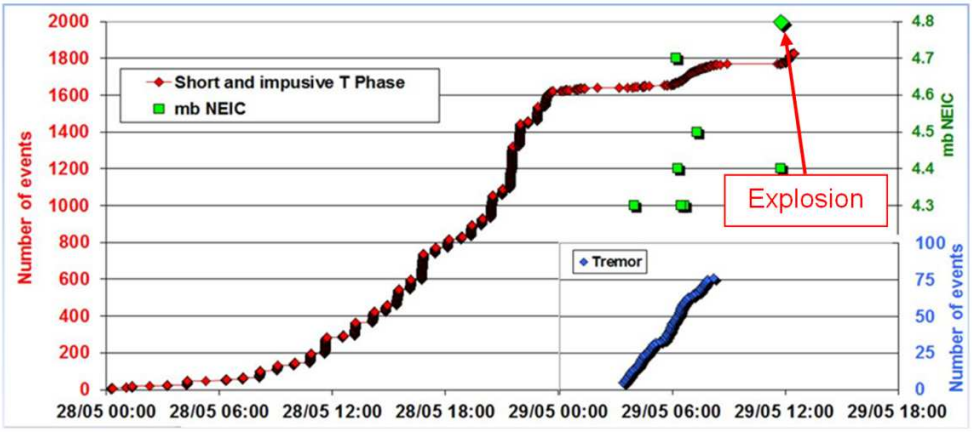

Figure 3: Histogram of the South Sarigan crisis based on records of the H11N1 (Wake IMS network) a very sensitive and well located hydrophone to monitor this underwater volcano. The events located by the ISC are shown in green with their magnitude (scale on the right). About 2,000 events have been selected. The brief and impulsive events (amplitude greater than 2 Pa and duration less than 3 s.) from the propagation of cracks during magma ascent towards the surface are shown in red (bottom left), and the tremors directly generated by the May 29th submarine eruption in blue (bottom right). Examples of these two types of events are shown in figures 4a and 4b (See Section 2.2 for details on event detection/classification).

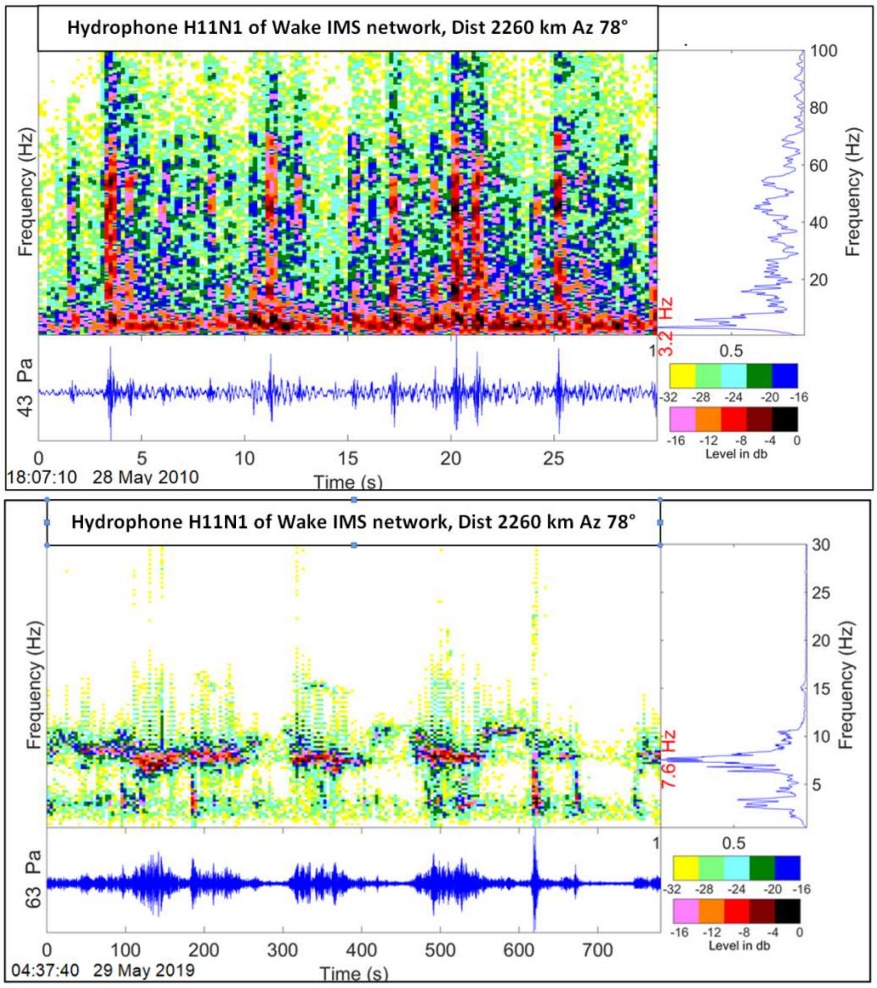

Figure 4: Typical examples of H11N1 (Wake IMS network) hydrophone records. a: Series of times and frequency spectra of a typical sequence corresponding to short and impulsive *T* phase (Figure 3). These very short signals (crack opening) were accompanied by continuous tremors (due to the difficult ascent of magma through cracks) with a maximum energy of c. 3.2 Hz. b: Tremors generated by the submarine eruption were similar to eruptive bursts recording of a hydrophone located 100 m away from the source of NW Rota-1 (Chadwick and al., 2008).

2. Waveform data and analysis

2.1. Seismic data and refined source location of the May 2010 paroxysmal explosive event

From the *Pg, Pn, P* and *T* phases recorded by numerous seismic or hydroacoustic stations in and around the Pacific Ocean, we carried out a multiphase location procedure (Talandier et al., 2002; Reymond *et al*., 2003; Talandier, 2004; Talandier and Okal, 2004) mainly based on the *T* phase data, that are in greater number and of better quality than the others. The adjustment of the epicentre uses a variable sound-speed in the channel SOFAR and the travel time takes into account the mean velocity along the path of the wave. Sound-speeds were defined according to the Levitus table which provides an annually-average speed by square of 1 degree. Figures 6 and 7 show these recordings of *T* phases (from the paroxysmal explosion of 29 May at 10:47 UTC) as (1) time records allowing precise determination of the times of arrival (lower diagram), (2) spectrograms showing the level (in dB by steps of 4 dB) of the spectral amplitude as a function of time (upper diagram) and finally (3) frequency spectra of the whole sequence in a linear scale (on the right). High-pass filtering improved the signal to noise ratio by eliminating the components lower than 2 Hz that are not propagated in the SOFAR channel. A correction taking into account the difference in travel time in the liquid and solid mediums was finally applied using a refined model of Hawaii (Hill, 1969; Watts and ten Brink, 1989). Two locations were finally obtained:

- with the *T* phases only (35 arrival times): 16.591° N, 145.764° E, at 11:47:46.79 UTC, Rms: 1.34;
- with the whole data (56), including 35 *T* phases (distances to the source of 2060 to 8300 km), 18 *P* (distances to the source ranging from 2,300 to 10,600 km) and 3 *Pg* or *Pn* (distances to the source of 12, 28 and 350 km): 16.596° N, 145.766° E at 11:47:47.90 UTC, Rms: 1.33.

The precision of the latter location was investigated through a Monte Carlo algorithm by carrying out a large number of relocations after injecting Gaussian noise with standard deviation σ_G into the dataset. We took $\sigma_G = 1.3$ corresponding to the standard deviation of the residuals broad value taking into account the quality of the data and association of *Pg*, *Pn, P* and *T* phases. The results for 1,000 iterations are shown in figure 5. The solution is remarkably robust, with a 1.5 km axis of the best-fitting ellipse. The location of this well constrained epicentre does not differ significantly from that deduced from the *T* phases only, a feature suggesting that the emission point of the *T* phases is very close or identical to the source of the seismic phases. Figure 5 shows that it corresponds closely to the volcanic edifice located c. 13 km south of Sarigan island. The best-fitting ellipse includes the crater shown in the National Oceanic and Atmospheric Administration (NOAA) post-eruption multibeam bathymetric map (Searcy, 2013) and considered as generated during the 2010 eruption (Embley et al., 2014). Although carried out with a large number of *Pg*, *Pn* and *P* phases, the locations of the International Data Center (IDC), National Earthquake Information Center (NEIC) and International Seismological Center (ISC) are c. 35 km away from the South Sarigan crater. This demonstrates the superiority of multi-phase locations in oceanic environments, with a preponderance of *T* phases combining a low propagation speed with exceptional detection power.

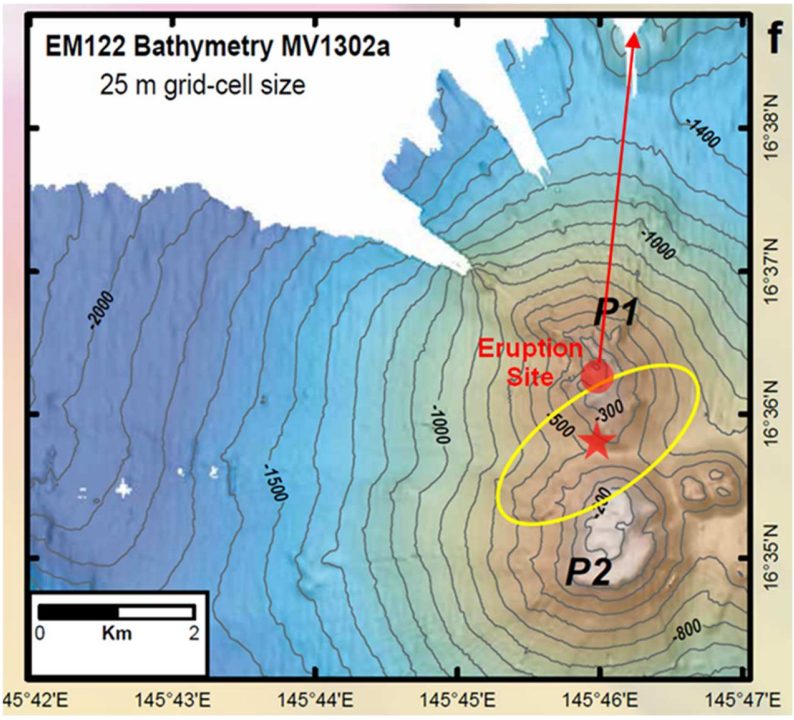

Figure 5: Multiphase location (56 *Pg, Pn, P* and *T* data) of the South Sarigan explosion shown as a red star on the bathymetric map of Embley et al. (2014). The epicentre position is well constrained with a major axis of the best-fitting ellipse (yellow) of approximately ± 1.5 km. The red circle marks the eruption site according to Embley et al. (2014). The red arrow indicates the direction of the point of reflection of the hydroacoustic wave on a seamount located c. 7 km north of this site.

2.2. Hydroacoustic data

Together with the channelling efficiency of the Sound Fixing and Ranging (SOFAR) channel, the all but negligible anelastic attenuation in the water column makes for an exceptionally efficient transmission of *T* phase energy at teleseismic distances and thus results in superb detection capabilities (Talandier and Okal, 1998; 2016)) for natural or artificial explosions, earthquakes, volcanic activity (Talandier and Okal, 1984; 1987), hydrothermal activity (Talandier and Okal, 1996) and iceberg drifting (Talandier et al., 2002; 2006). In such cases, *T* phases can be recorded either by island seismic stations after conversion of the acoustic wave to seismic wave on the underwater slopes or by hydrophones wetted in the SOFAR channel. In this paper, all displayed records were corrected for the instrumental response and a high-pass filter improving the signal/noise ratio by eliminating the components lower than 2 Hz that are not propagated in the SOFAR channel. The location of the Wake network hydrophones is shown in Figure 2 (HA11 North and South triplets). Their mooring depth (1,200 m) is close to the axis of the SOFAR channel. The sampling frequency is 250 Hz with high recording dynamics (Lawrence, 2004; Harben and Hauk, 2010). Masked by a seamount, the southern network (H11S) recorded poorly the hydroacoustic waves of the South Sarigan explosion (Green et al., 2013). We will therefore use only the recordings from the northern network (H11N) from which all the recordings of the crisis have been acquired. About 2,000 events of amplitude greater than 2 Pa were selected.

2.2.2. Paroxysmal explosion of 11:47 UTC

The record of the *T* phase of the 11:47 UTC paroxysmal explosion by the network hydrophone H11N1 is shown in Fig. 6. Three well defined arrivals were separated by 5 to 6 s. The first one (a), of small amplitude, was related to an initial propagation in the solid medium towards a point of remote conversion of the source. It was followed by the direct *T* phase (b), and then by a wave (c) reflected on a seamount 7 km north of the epicentre (red arrow in Fig. 5). The poorly defined start of the waves (a) and (c) does not allow us to show a change of azimuth of these two phases relative to the main wave (b). A zoom on the direct *T* phase (Fig. 7) shows a short and intense a short and intense *T* phase (1700 Pa) whose growth on a split second characterizes an impulsive and fast source. As discussed below (see Fig. 14), the amplitude growth is exceptionally fast relative to the average *T* phase from underwater explosions. At 2,300 km a beginning inverse dispersal of frequency (i.e. decreasing frequency variation as a function of time: Talandier and Okal, 2016) is observed. We note the contrast between this very high amplitude (1700 Pa) of the *T* phase generated by the final paroxysmal explosion and those corresponding to the explosive magmatic activity in Figure 4b (60 Pa). The *T* phase recorded by the seismic station of Canton Island (KNTN) also displays direct and reflected waves (Fig. 8), separated by a 5 s gap similar to that recorded by the Wake hydrophone. At more than 5,000 km away, the inverse frequency dispersal characteristic of an explosive source (Talandier and Okal, 2016) is well developed.

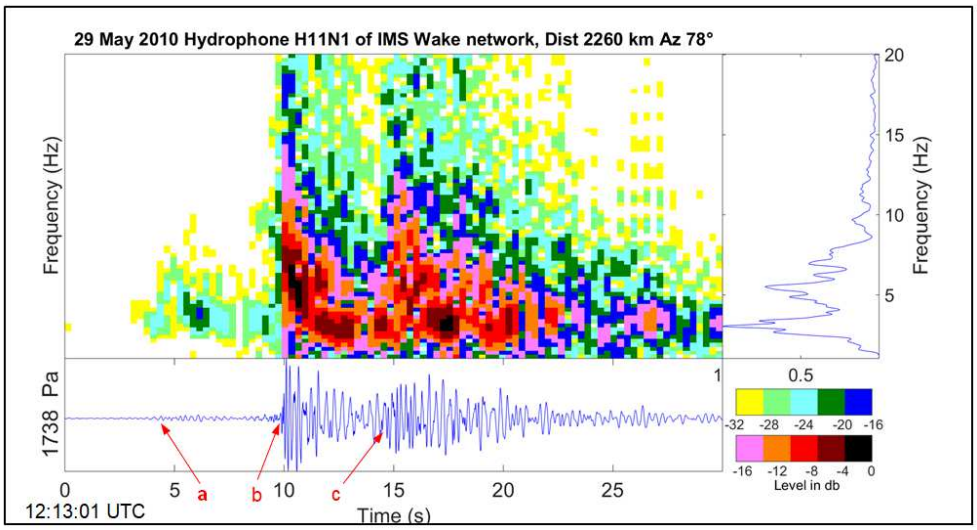

Figure 6: Example of standardized processing of *T* phase record of the 11:47 paroxysmal explosion. The bottom plot shows a 30 s window of the pressure time series. The frequency spectrum of the whole sequence is shown to the right of the main plot, which is a spectrogram representation of the distribution of spectral amplitudes as a function of time and frequency. The colour coding is logarithmic, with the key (in decibels relative to the most energetic pixel) given at bottom right. Three well defined arrivals were separated by 5 to 6 s. The first one (a), of small amplitude, was related to an initial propagation in the solid medium towards a point of remote conversion of the source. It was followed by the direct T phase (b), and then by a wave (c) reflected on a seamount 7 km north of the epicentre (red arrow in Fig. 5). As for the other figures, the azimuth is that of the source to the receiver deduced from their locations.

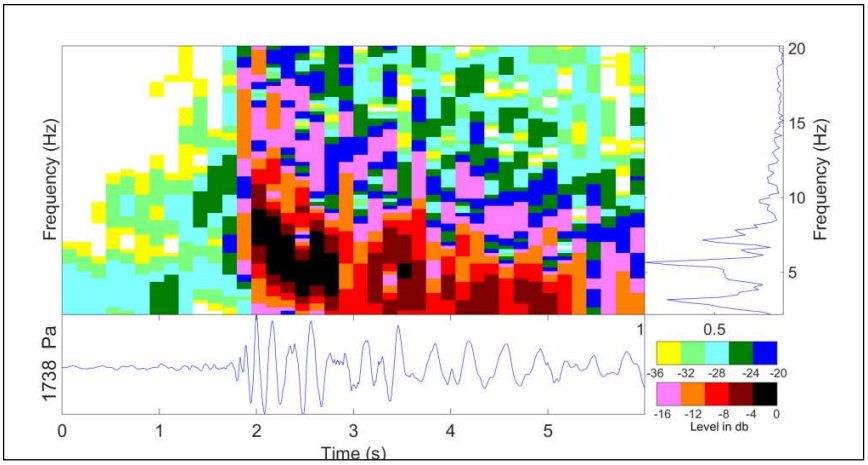

Figure 7: Zoom on the *T* phase of figure 6 whose growth on a split second characterizes an impulsive and fast source. The amplitude growth is exceptionally fast relative to the average *T* phase from underwater explosions (see Fig. 14 below). At 2,300 km a beginning inverse dispersal of frequency is observed (Talandier and Okal, 2016).

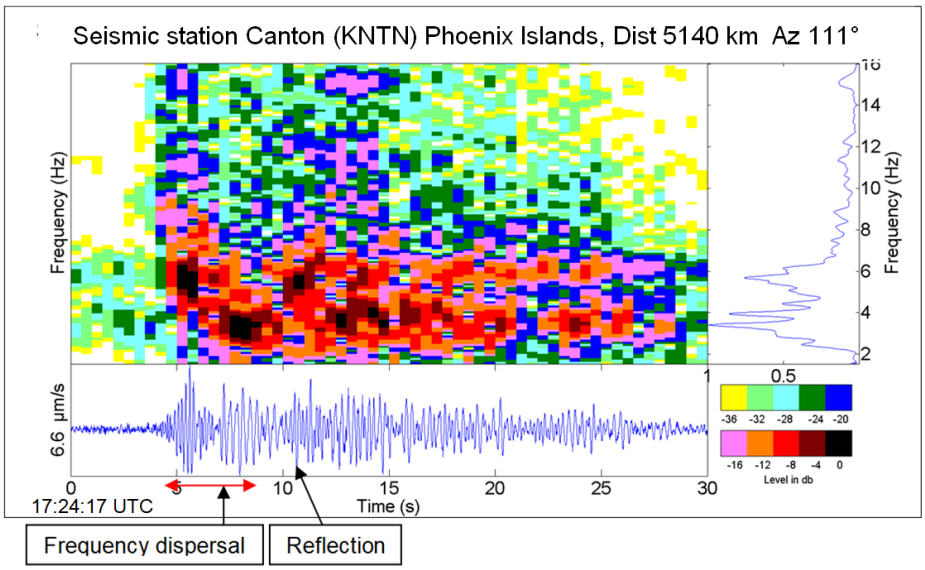

Figure 8: The *T* phase of South Sarigan explosion recorded at Canton (KNTN) seismic station. High-pass filtering improves the signal/noise ratio by eliminating the components lower than 2 Hz that are not propagated in the SOFAR wave guide. The direct and reflected waves identified on the hydrophone of Wake are separated by the same time gap (5 s). At more than 5,000 km the inverse frequency dispersal is well developed.

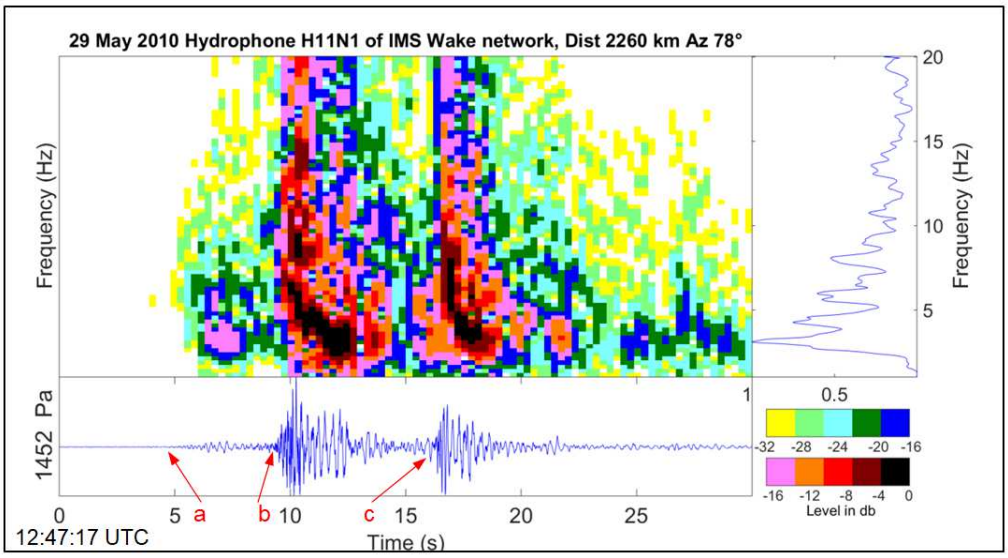

Figure 9: *T* phase of 11:59 UTC explosion. The slightly higher difference (relative to the 11:47 explosion) between the direct and reflected waves on the seamount north of South Sarigan may indicate that the 11:59 explosion occurred further away, but this hypothesis cannot be confirmed because of its poorly constrained location.

2.2.2. Explosion of 11:59 UTC

The H11N1 *T* phase record of the 11:59 UTC explosion that followed the 11:47 paroxysmal explosion is shown in Figure 9. Although it is clearly identified as an explosion, its location is poorly constrained based on only 12 data (*P* & *T*) with a major axis of the best-fitting ellipse of ± 3.0 km, (16.605° N, 145.756° E at 11:59:02.44 UTC) and therefore cannot be differentiated from that of the 11:47 using 18 *P* and 35 *T* phases. Rather emergent, the beginning of the corresponding *T* phase suggests a source less fast and impulsive than the 11:47 explosion. The fact that only a few stations recorded this 11:59 event suggests a much lower energy release compared to the 11:47 paroxysmal explosion, and being isolated it cannot be associated with eruptive activity. It might correspond to a small phreatomagmatic explosion, but this hypothesis is presently not supported by other kinds of informations.

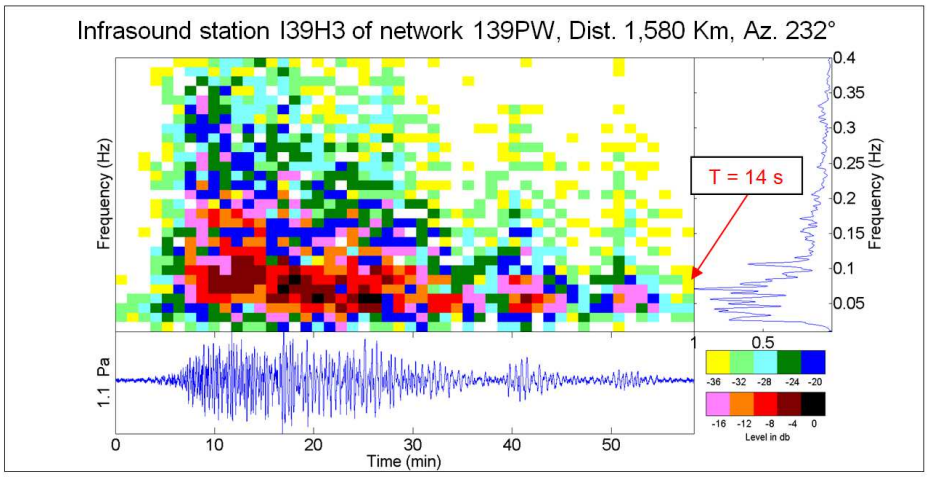

Figure 10: Infrasound recording at I39H3 station of Palau IMS network, 1,580 km away from South Sarigan. High-pass filtering improves the ratio signal noise by eliminating the components lower than 0.03 Hz. Infrasound sequences of long duration (50 minutes) are constituted by multiple tropospheric and stratospheric arrivals.

2.3. Infrasound data

Palau Island IMS network, located 1,580 km ESE of South Sarigan, recorded the infrasounds of the paroxysmal explosion, that were studied in detail by Green and al. (2013). Their 50 minutes long sequence (Fig. 10) is constituted by more or less overlapping multiple arrivals, in agreement with the results of Fee et al. (2013) who showed that distant infrasound records involve multiple tropospheric and stratospheric inseparable arrivals. Infrasound related to three explosions of the subaerial Kasatochi volcano (Prejean and Brodsky, 2011; Arnoult et al., 2010; Fee et al., 2010) were recorded by I53 station in Alaska and I44 station in Kamchatka located 2,150 and 1,730 km away from the source, respectively.

2.4. Tsunamis

The Saipan tide gauge located 156 km south of the explosion site recorded two successive tsunamis (Fig. 9). The first one occurred at 12:15 UTC, and was characterized by a period from 15 to 30 min, an amplitude of 3 cm and a propagation time of 28 minutes compared to 25 minutes for the simulation shown in Figure 13. This 3 minutes difference may be due either to a short delay in the formation of the tsunami after the explosion (the triggering of the tsunami was likely not instantaneous and, although negligible at long ranges, this time must be taken into account for a receiver located at only 156 km away from its source) and/or to an error introduced by too coarse a computing grid.

A second tsunami occurred 01:45 hour after the explosion, at 14:00 UTC, with an amplitude (6 cm) and periods (30 to 40 minutes) greater than those of the first one, but was not correlated to any acoustic, hydroacoustic or seismic signal except a probably superficial seismic wave of weak amplitude and low frequency (0.5 Hz and almost monochromatic, Fig.12), recorded in the immediate vicinity of the

eruption site (SARN at 13 km). Exceptionally long periods for a tsunami of such low energy and lack of high frequencies (*Pg*, *P* and *T*) characterize a very slow source. Slow source as in the case of tsunami-earthquakes resulting from an exceptionally slow rupture velocities rupture with also marked body wave deficiency (Newman and Okal, 1998; Okal et al., 2003). Unlike those of NW Rota-1 studied by Chadwick et al. (2012), the second South Sarigan tsunami was not triggered by a submarine volcanic eruption, and therefore might rather be considered as an indirect consequence of the 11:47 UTC paroxysmal explosion.

,

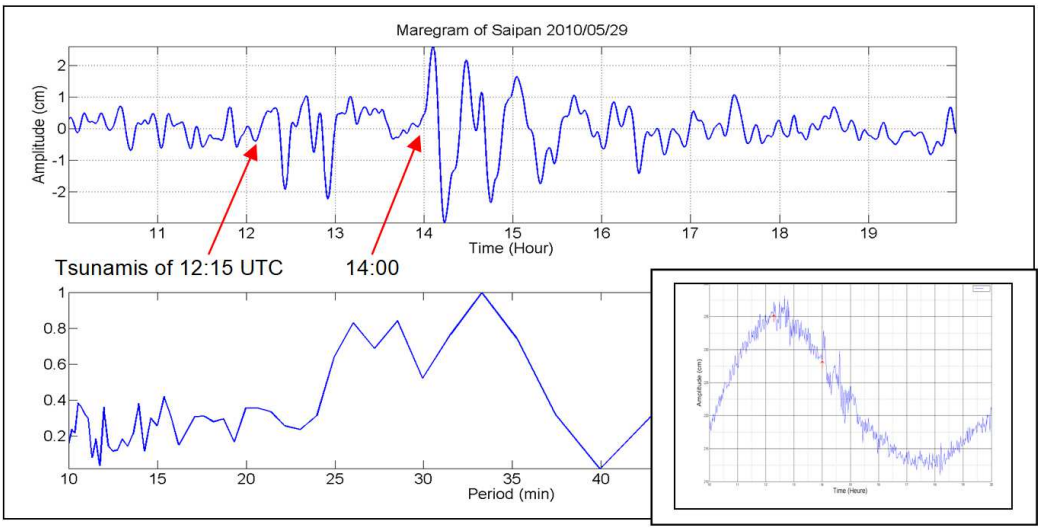

Figure 11: Records of Saipan tide gauge, 156 km away from the explosion, filtered between 360 and 6,000 s. The original records are shown in the bottom (right) plot. Two tsunamis with well-defined arrivals at 12:15 and 14:00 UTC, respectively, were observed. The first one was well correlated with the 11:47 UTC explosion and was probably a direct consequence of this event. The second one, of greater amplitude and periods than the first, was not correlated with any hydroacoustic signal. However, a seismic wave of weak amplitude and low frequency (0.5 Hz and almost monochromatic), probably a superficial wave, was observed in very near field (SARN, 12 km away from the source; see Fig. 12).

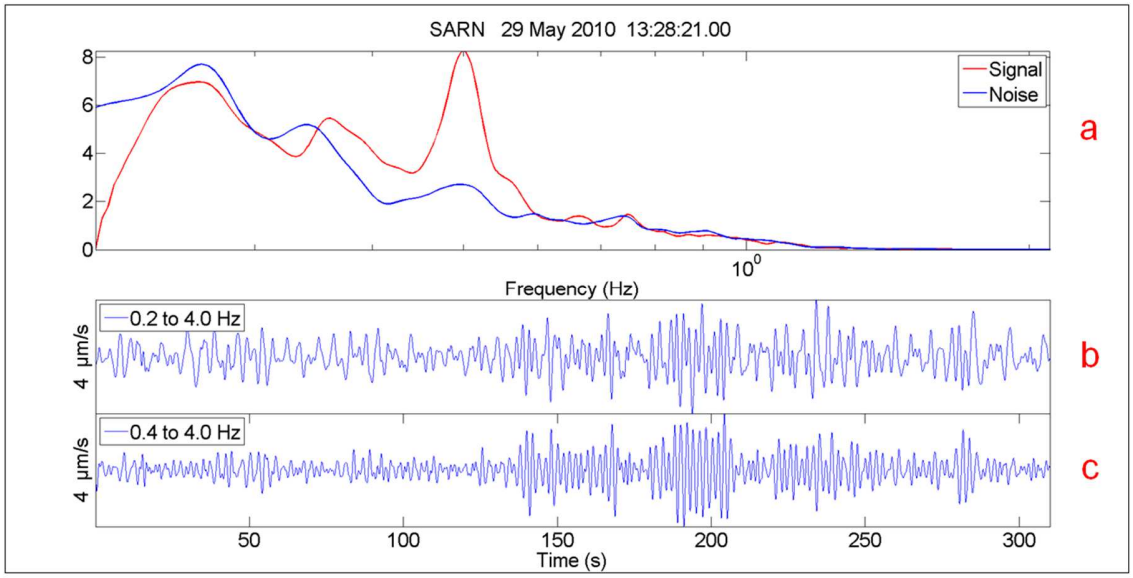

Figure 12: Seismic signals of SARN (Sarigan island), located 13 km away from the source of the 14:00 UTC tsunami. After correcting for the instrument response of the seismic chain the bandwidth is extended until a period of 0.1 Hz. a: signal sequence filtered between 0.2 and 4.0 Hz (in red) and noise spectra (in blue); b: time series filtered between 0.2 and 4.0 Hz; c: time series filtered between 0.4 and 4.0 Hz. The superficial wave at 0.5 Hz is clearly above the microseismic background noise.

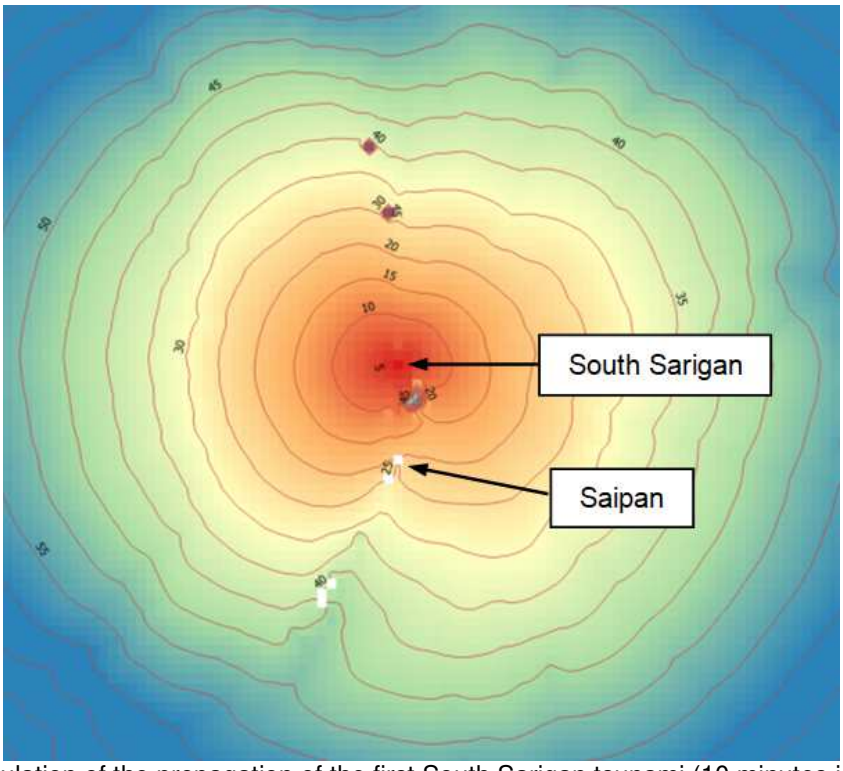

Figure 13: Simulation of the propagation of the first South Sarigan tsunami (10 minutes isochrons). We note the high incidence of islands and seamounts. The modelled propagation time is 25 minutes compared to 28 minutes for the time observed. This difference of 3 minutes may be due to the delay in the formation of the tsunami and by using too coarse a computing grid.

3. Yield estimation and tentative explosion scenario

3.1. Identification criteria for the source of T phases

The enforcement of the Comprehensive Nuclear-Test Ban Treaty (CTBT) requires the monitoring of acoustic sources in the oceans in order to detect underwater explosions. Criteria of identification of the nature of the sources of the *T* phase are described in several papers based on the Polynesian Seismic Network (RSP) data (Talandier and Okal, 1987, 2001; Reymond et al., 2003; Talandier and Okal, 2004; Talandier et al., 2013; Talandier and Okal, 2016). These criteria can be applied to records from both hydrophones and "*T* phase" seismic stations. In the time domain, and in addition to the classical duration-amplitude discriminant, we use a catalogue of reference envelopes to which a signal can be directly compared by cross-correlation algorithms. In the frequency domain, we use several methods including the study of the decay of spectral amplitude with frequency (both in terms of a power law, and of

smoothness), and the evolution of the duration of the signal when corrected using an empirical compensation of any frequency dispersion present in its Fourier spectrum. The combination of these methods provides a precise identification of the nature of all sources with reference to a large dataset of more than 300 signals. The paroxysmal explosion of May 29th, 2010 at South Sarigan is exceptional because of its energy and the fact that it affected at the same time solid, liquid and subaerial media. Therefore, it gives us the opportunity to apply these criteria to the *T* phases of South Sarigan recorded by the Wake hydrophone H11N1 and KNTN seismic station. In order to illustrate the application of these criteria, in addition to the treatment of the the South Sarigan explosion *T* phases records of stations H11N1 (Fig. 14) and KNTN (Fig. 15) we show in figure 16 that of an artificial underwater explosion.

(a) Duration-amplitude criterion (Talandier and Okal, 1987, 2001, 2016):

We measure the maximum e_{Max} of the envelope of the ground velocity recorded in the *T* phase at the receiving station (in μm/s) and the duration $\tau_{1/3}$ during which the envelope is sustained at or above 1/3 of e_{Max} (in seconds).

The quantity $$D_0 = \log_{10} e_{Max} - 5.0 \log_{10} \tau_{1/3} + 4.53 \qquad (1)$$

can act as a discriminant effectively separating explosions ($D_0 > 0$) from earthquakes ($D_0 < 0$).

If, after application of the other criteria, there is still doubt concerning the identification of the source, a more complex relationship involving measurement of duration before and after compensation of inverse frequency dispersion may be used. In the present case, the different criteria converge to identify the South Sarigan event as an explosive source. As shown on figures 14 and 15 the D_0-values of 1.6 and 3.6, respectively for hydrophone H11N1 and KNTN seismic station, clearly identify an underwater explosion. As shown in Figure 16, these results are consistent with the D_0-value of 3.3 obtained for the artificial Vanvouver underwater explosion (Talandier and Okal, 2004).

(b) Identification of frequency dispersal inversions (Talandier and Okal, 2016):

The *T* phase station records from explosive sources in the water column feature a systematic inverse dispersion, with lower frequencies traveling slower, which is absent from signals emanating from other sources. We have developed an algorithm to compensate this frequency dispersion. Associated with amplitude growth, the duration measurement on the signal envelope before and after compensation identifies explosive sources. In figures 14 to 16, decrease in duration and increase in amplitude effectively identifies an explosive source.

(c) Reference envelope and time of rise (Talandier and Okal, 1987, 2001):

This criterion is based on the measurement of the maximum of the envelope of the ground velocity recorded in the *T* phase at the receiving station and the duration 1⁄3 during which the envelope is sustained at or above 1/3 of this maximum. Four reference envelopes can be considered: i) subduction zone earthquake, ii) intraplate-type earthquake iii) explosive event during a volcanic swarm, and iv) artificial underwater explosion. In figures 14 to 16, the envelope of the *T* phase is shown in green (or in red in Figs 14a, 15a and 16a), while the reference envelope for an artificial underwater explosion is shown in blue. The width of the South Sarigan *T* phase envelope is smaller than that of the artificial reference

envelope and its amplitude growth (red dotted line) is clearly faster. Therefore, the source of the South-Sarigan event is typically explosive and at least as impulsive and fast as those of artificial underwater explosions.

(d) Study of the decay of spectral amplitude with frequency (Reymond et al., 2003):

Both in terms of a power law f^2 and of smoothness α, earthquakes and explosions can be discriminated on the basis of the variation with frequency of the spectral amplitude of ground velocity. A dataset of 206 records indicates that for most explosions $\alpha < 1.4$, while most earthquakes have $\alpha > 1.5$. Moreover, the correlation coefficient f^2 is generally smaller than 0.7 for most explosions, and greater than 0.75 for most earthquakes. However, the f^2 coefficient is essentially conditioned by the presence or absence of bubble pulsation, i.e. modulation of the frequency spectra by contractions and dilations of a bubble during its ascent towards the surface of the ocean (Cole, 1948; Wielandt, 1975), as illustrated by the artificial explosion (Fig.16). The rather regular shape of the South Sarigan spectra is inconsistent with a bubble effect. This conclusion is consistent with the lack of any bubble-generated peak in the hydrophones H11S1 and H1N1 records as well as in the KNTN seismic station data. The source of South Sarigan event being impulsive and fast, the observed strong spectral decay would be in agreement with a large size volcanic source rather than a punctual man-made underwater explosion.

In short, the application of various discrimination criteria used for hydroacoustic sources to the *T* phase generated by South Sarigan event of 11:47 UTC leads to the obvious conclusion that it derived from an impulsive source, similar in many respects to a submarine shot. The natural (i.e. volcanic) origin of this underwater explosion of strong energy not contained in the water is consistent with the absence of pulsation of a bubble and the deficiency of high frequencies relative to the frequency spectra of the *T* phases of submarine shots.

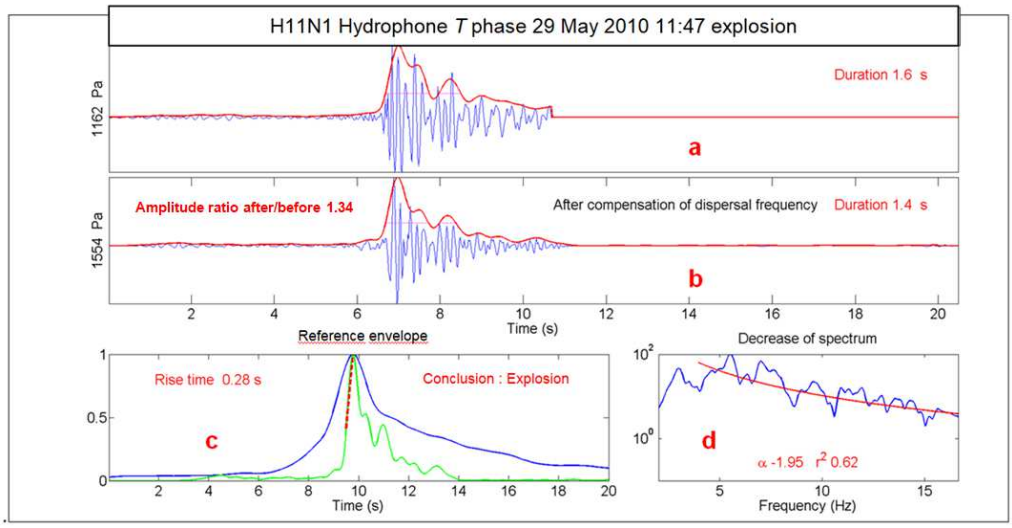

Figure 14: Application of identification criteria to the H11N1 *T* phase of the South Sarigan paroxysmal explosion. The amplitudes of the direct *T* phase are normalized at a distance of 3,000 km.
a) Duration-amplitude criterion: plots of the time series within the reference envelope, showing the maximum peak-to-peak amplitude (left) and the duration measured on the envelope at the third of its maximal amplitude (top right).
b) Identification of the dispersal inversions of frequency: plots of the signal compensated for a possible dispersal of frequency, showing maximum peak-to-peak amplitude after compensation (left), the relationships between the amplitude before and after compensation (top left) and the duration after compensation (top right).
c) Criterion of the reference envelope and the time of rise: plots of the signal envelope and the reference envelope adjusting at best, showing the time measure of rise (on top and left) and the event category corresponding to this criterion (top right). The reference envelope for explosive sources is shown in blue, and that of the South Sarigan *T* phase in green or red. The width of the South Sarigan envelope (in green) is smaller than the smaller explosion reference envelope, and the amplitude growth of the South Sarigan *T* phase (red dotted line) is clearly faster than the reference one.
d) Study of the decay of spectral amplitude with frequency: α denotes a power law, and r^2 the smoothness. The high value of the coefficient r^2 denotes the lack of bubble pulsation.

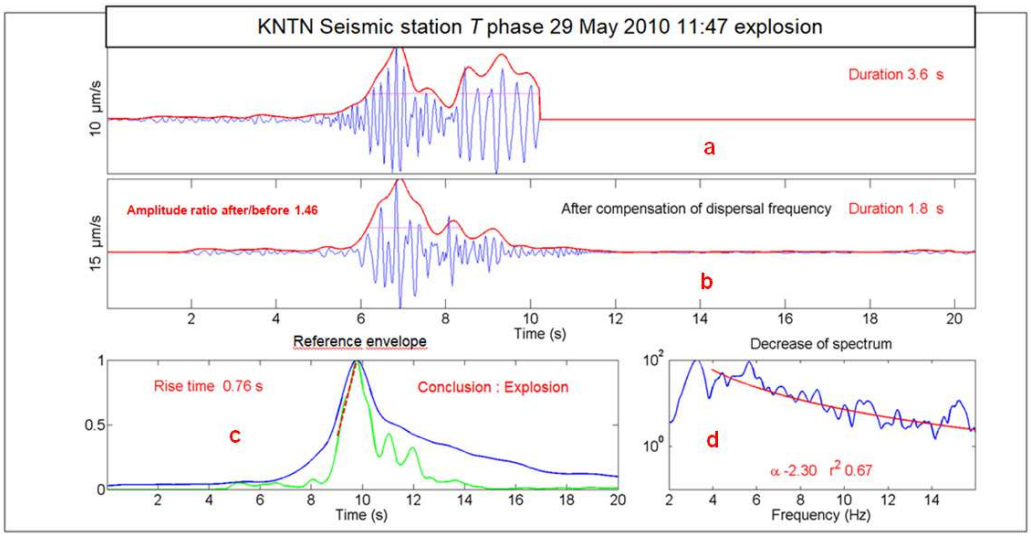

Figure 15: Application of identification criteria to the KNTN seismic *T* phase recording of the South Sarigan paroxysmal explosion. Conventions as in figure 14. With respect to the recording of hydrophone H11N1, the amplitude ratio before/after compensation and amplitude growth are higher (Figs 15a and 15b) due to a greater distance to the source. This criterion is also fulfilled for higher rise time and duration (Fig. 15c). The high value of the r^2 coefficient shown in figure 15d is also consistent with a lack of bubble pulsation.

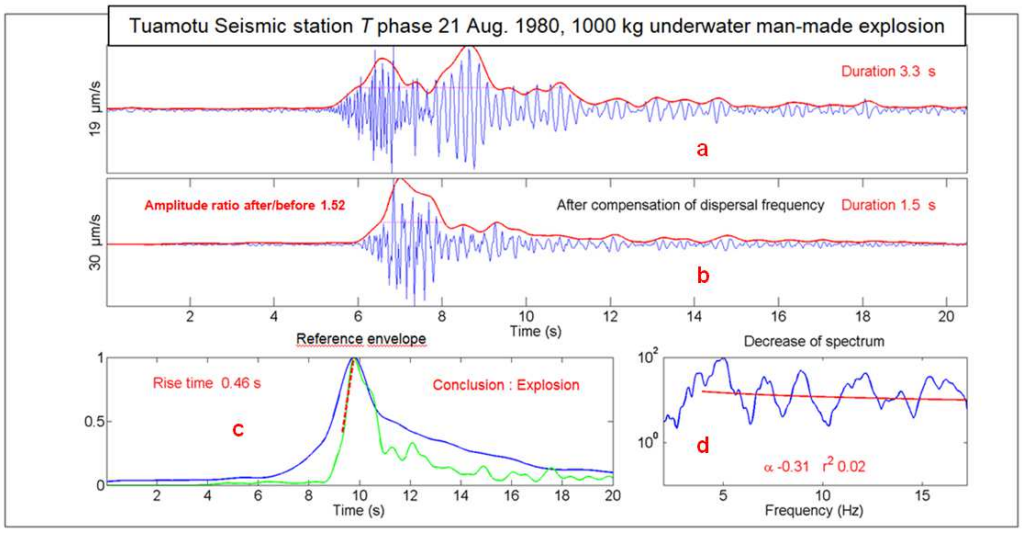

Figure 16: Application of identification criteria to seismic station *T* phase of the Vancouver artificial explosion of 1,000 kg of TNT. Conventions as in figure 14. The data shown in figures 16 a, b and c are typical of an explosive source similar to that of the South Sarigan explosion. However, the low value of the r^2 coefficient (Fig. 16d) indicates the occurrence of a bubble pulsation effect, phenomenon that is not documented for the South Sarigan explosion (Figs 14 and 15).

3.2. Application of discriminating criteria Ms versus mb

The application of the discriminating criteria magnitude Ms versus mb distinguishes the explosive and seismic sources (Aki et al., 1974). The magnitude mb deduced from the body *P* phases corresponds to the portion of elastic energy diffused in the solid medium. The magnitude Ms characterizes the superficial waves channeled into the earth's crust and upper mantle.

Different formulations have been proposed depending on the nature of the explosion environment (Liebermann and Pomeroy, 1969; Murphy and Mueller, 1971; Murphy and Baker, 2001). We will focus on the most recent one by Selby et al. (2012) and Ford and Walter (2014) who define a boundary separating seismic sources from explosive sources:

$$Ms < mb - 0.64 \qquad (2)$$

This relationship yields a magnitude of mb = 4.7 (ISC) and Ms = 3.6 when applied to the South Sarigan explosion, and therefore supports the explosive nature of its source.

3.3. Estimation of released energy from seismic data with reference to nuclear tests

The explosion of South Sarigan volcano was initially reported as an earthquake by the IDC, USGS and NEIC. However, rather than a double couple seismic source, the similarity of the *P* phases with those of underground nuclear tests and the application of identification criteria for sources of *T* phases identifies without ambiguity an explosive source, at least as impulsive and as fast as a man-made explosion (Figs. 14 to 16). However, many databases (Brown, 2014; Gudmundsson, 2014) and estimates of the energy of

453 volcanic explosions (Hedervari, 1963; Mason et al. 2004; Vyacheslav et al., 2006; Rougier et al., 2018)
454 concern explosive eruptive activity and not, such as in the case of the South Sarigan paroxysmal event,
455 explosions clearly decoupled from the main eruptive crisis. Concerning the energies released, for
456 instance, the subaerial explosive eruptions of Kasatochi volcano in the Aleutian Islands (Waythomas et al.,
457 2010) and Augustine in Alaska (Prejean and Brodsky, 2011) involved the emission of ash plumes 10-18
458 km high, more or less similar to that of South Sarigan (12 km) which emerged after a transit of some 200
459 m in the water column. Seismic *Pn* phases about ten minutes long were recorded only in the field near the
460 volcanoes Kasatochi and Augustine, while a *P* phase only 10 seconds long was recorded in the far field of
461 South Sarigan. Chadwick et al. (2008) and Wright et al. (2008) studied the submarine crises of Monowai
462 volcano in the Kermadec archipelago (southeast Pacific). The *T* phases associated with the explosions of
463 this volcano were clearly different from the very brief and impulsive *T* phase of South Sarigan (Figs 6 and
464 7). These former sources, typical of volcanic explosions directly connected to an ongoing eruptive
465 process, differ essentially from the violent and impulsive explosion of South Sarigan.
466
467 The explosion of South Sarigan was not a precursor of a significant eruptive activity, but the final
468 consequence, differed by 3 h 30, of such magmatic activity. This event that affected concomitantly the
469 solid, liquid and subaerial media is presently the first well documented volcanic explosion, not associated
470 with eruptive magmatic activity, having generated intense waves: (*P*), hydroacoustic (*T*), acoustic
471 (Infrasounds) as well as tsunamis. The use of this exceptional event within the Comprehensive Nuclear-
472 Test–Ban Treaty (CTBT) framework needs an evaluation of the corresponding energy release. As its
473 source was buried, only its seismic effect could be representative of the released energy. The *P* phases
474 recording of the South Sarigan paroxysmal explosion is shown in Fig. 17. Its frequency spectrum,
475 characterized by a relatively impulsive onset and short duration (10 s), is typical of an explosive source
476 (Talandier and Okal, 1987, 2001, 2016). Its magnitude, $4.7 < mb < 4.8$, deduced from the *P* phases by the
477 ISC and NEIC, plots within the range of those of underground nuclear tests. Therefore, this feature allows
478 us to use relationships previously established for estimating the energy released by underground nuclear
479 explosions from their seismic effects, with all the reservations implied by the different nature of the
480 volcanic source. Note that the formalism of Newman and Okal [1998] would allow us to estimate the
481 elastic energy of these phases *P* but we do not have a similarity law to deduce the total energy released
482 by the source.
483
484 On the basis of 39 events concerning the most known test sites and their type of host rocks,
485 Marchal et al. (1979) and Bache (1982) defined low and high limits of magnitude versus yield
486 relationships:
487 $$mb_b = 0.73 \log(E\ kt) + 4.38 \qquad (3)$$
488 and
489 $$mb_h = 0.77 \log(E\ kt) + 4.08 \qquad (4)$$
490

With mb = 4.7 we obtain 2.7 kt with *(2)* and 6.4 kt with *(3)*. The average value of 4 kt nuclear blast is equivalent to 2 kt of TNT.

However, as the phenomenology of the South Sarigan volcanic explosion is clearly different from that of a chemical or nuclear explosion, the above result must be amended. Schematically, three forms of energy need to be taken into account for an underground explosion: mechanical energy that fractures and crushes the medium; elastic energy that is propagated in the Earth; and finally dissipated thermal energy. The mechanical and seismic effects induced by the shock are identical in the natural and artificial cases; according to several authors (e.g. Cole, 1948), they represent half of the total released energy. The other half corresponds to thermal effects trapped within the fireball that are of course much weaker for a volcanic explosion. Therefore the energy contained in the shock linked to South Sarigan explosion can be evaluated to about 1 kt (corresponding to energy of 4.2×10^{12} J on the basis of 4.2×10^{3} J/g).

This conservative evaluation is probably on the low side of the energy range involved. Indeed, South Sarigan explosion was certainly much shallower than most underground nuclear explosions. Murphy and Mueller (1971) showed that the elastic energy efficiencies increase with the depth of burial according to a law of the form $h^{0.72}$. This could imply an underestimation of our result by a factor of 2 or 3. Moreover, the young and shallow andesitic volcanic bedrock of South Sarigan is probably more heterogeneous and less coherent than those of nuclear test sites, a feature that moves in the same direction. Finally, the proposed estimate relates only to the portion of released energy corresponding to the observed seismic effects. It does not take into account the hydroacoustic effects and the violent ejection of materials into the water column and the atmosphere.

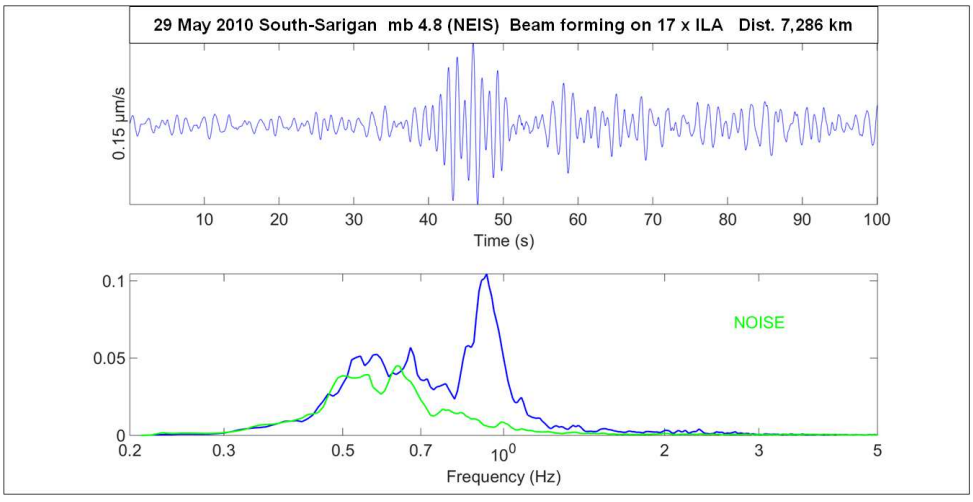

Figure 17: *P* phase record of the South Sarigan paroxysmal explosion (Beam forming on 17 stations of the Yellowknife network). The microseismic noise is shown in green. See text for explanations.

3.4. Evaluation of hydroacoustic effects with reference to T phases of artificial underwater explosions

Taking into account a wide range of artificial underwater explosions, among which the ITRI experiment (in 1968: 340 t) in the Aleutian Islands, and the CHASE series of 5 explosions (ranging from 53 to 346 t) in 1969 and 1970 off Vancouver Island (Talandier and Okal, 2004; Talandier, DASE/LDG Hydroacoustic seminar, May 2008), we concluded in a progress in W^{c1} for the relations connecting the intensity of the hydroacoustic signals with the charge of these explosions. The value of $c1$ = 0.65 is consistent with the theoretical study of Wielandt (1975) who described explosions in terms of 'volume of the source', a parameter that varies with time.

The regression of our data leads to the following relationship between hydroacoustic signals and the order of magnitude of explosive charges:

$$\log (Amp) = c1 \times \log (Cha) - c2 + \log (Pro / 200) \qquad (5)$$

The charge (*Cha*) is in kg of equivalent TNT, the amplitude (*Amp*) in µm/s peak to peak normalized at a distance of 3000 km and (*Pro*) the depth of the explosion in m. However, if the coefficient *c1* characterizing the slope of the regression line is well defined, conversely, depending on the dataset used, the coefficient *c2* can be scattered. Therefore, we will take into account its lowest and highest values, which lead us to obtain an order of magnitude of the energy released.

For the explosion of South Sarigan we obtain:

Station	Distance (km)	Azimut (°)	Amplitude (µm/s)	Charge (kg)	Charge (kg)
				$c2_b$ = 0.60	$c2_h$ =1.1
KGM	2165	304	18	383	2252
WAKE	2230	79	15	302	1777
KNTN	5106	111	7	267	1568
BNB	8055	39	6	356	2093
			Mean	327	1923

The distribution of azimuths does not highlight any directive effect of the source. However, as the efficiency of the acoustic/seismic conversion is dependent from numerous factors (e.g. the position of the station with respect to the coast and the submarine slope dip), the scatter is rather large. We will retain an average value of about 1000 kg of equivalent TNT. However, given the very high intensity (1700 Pa) of hydrophone recordings at H11N (Figures 6 and 7), this value of 1000 kg seems to be underestimated. This disagreement between the amplitudes of seismic and hydrographic stations is partly due to the very impulsive beginning of the *T* phase involving high frequency components that seismographs cannot record.

548 The hydroacoustic effects of the South Sarigan explosion are therefore similar to those of man-
549 made underwater explosions of ca 1t equivalent TNT, i.e. one thousand times smaller than the energy
550 deducted from the *P* phase (1 kt). Two successive stages must therefore be considered. The first (and by
551 far major one from the point of view of energy release) occurred in a shallow magmatic chamber. Its
552 strong magnitude (ISC 4.7, NEIC 4.8) was similar to those of underground nuclear explosions. The
553 second stage occurred when the internal pressure exceeded the resistance of the top roof of the
554 submarine volcano. The rise of amplitude in a fraction of a second of the *T* phase on the Wake
555 hydrophone and its duration lower than one second are consistent with a very strong and violent
556 decompression. We found no other example in distant field of such a brief and impulsive *T* phase.
557
558
559
560
561
562
563

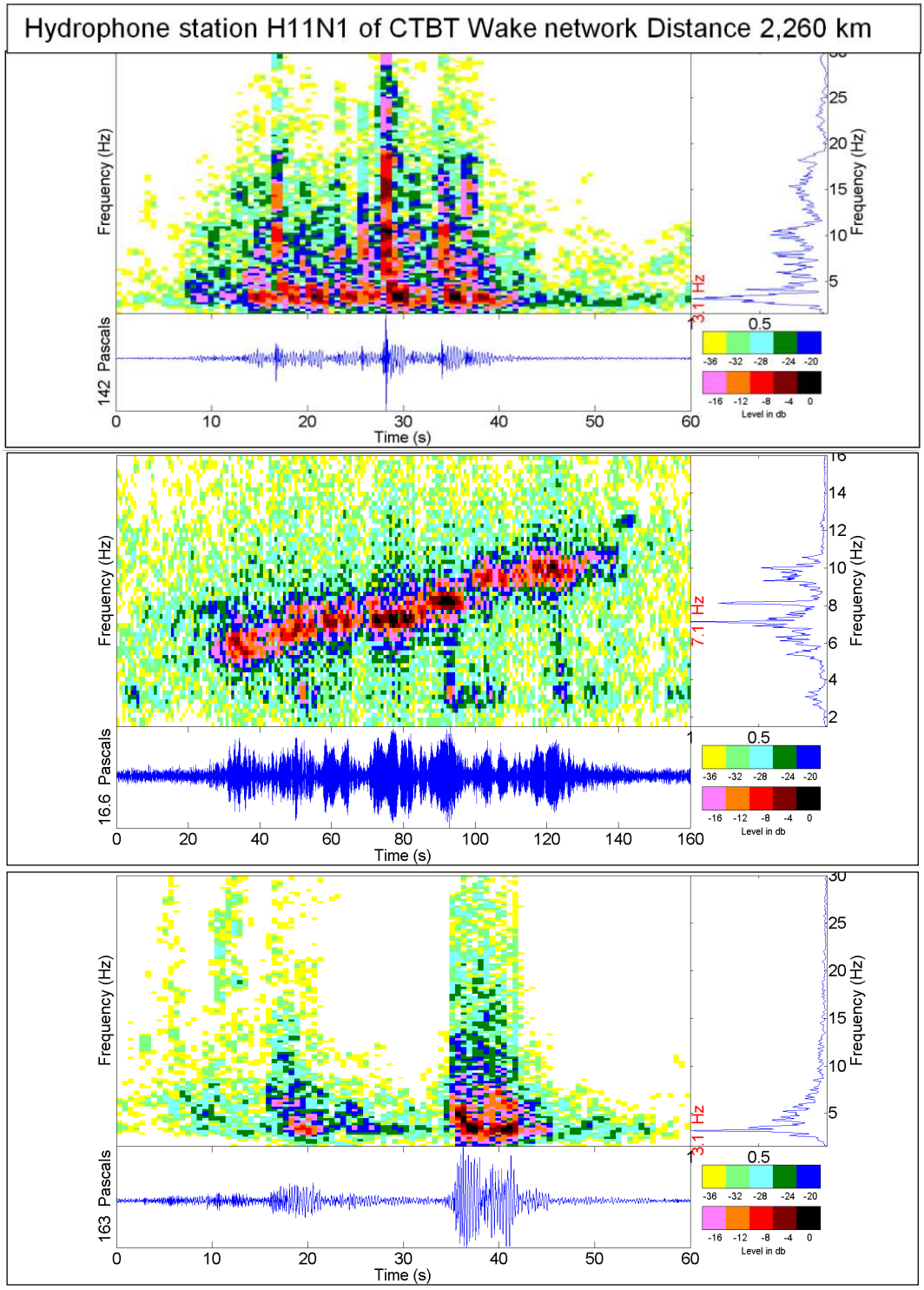

564

565

566

567 Figure 18: The three tremors observed at UTC 11:39:20, 11:43:41 and 11:46:31 (respectively 08' 27", 04'
568 06" and 01' 15" before the explosion). Following a 3 h 30' gap of any observable activity, they were clearly
569 different from those directly generated by the submarine explosion (Fig. 3). The rather intense first one
570 was associated with some small punctual explosive events. The second one was characterized by an
571 almost linear frequency increase from 5.5 to 10.5 Hz in 120 s. The last one, very close to the final
572 explosion, could indicate a weakening of the cavity roof.

3.5. Explosion process: a tentative scenario

A very specific tremor, characterized by an almost linear frequency increase from 5.5 to 10.5 Hz in 120 seconds (Fig. 18) occurred four minutes before the explosion and 3 h 30 after a full cessation of observable activity. Similar sliding frequency tremors preceding explosive eruptions have been studied by Jellinek and Bercovici (2011), and observed in Soufriere Hills, Montserrat (Powell and Neuberg, 2003), Arenal, Costa Rica (Lesage et al., 2006) and Redoubt, Alaska (Hotovec et al., 2013). However, major differences between these tremors and those of South Sarigan lie in their exponential variations of frequency on long durations, (10 to 20 minutes), and the presence of harmonics, while in South Sarigan the frequency sliding was almost linear and of clearly shorter duration (2 minutes) without any detectable harmonic. All proposed mechanisms (Powell and Neuberg, 2003; Lesage et al., 2006; Hotovec et al., 2013) involve an increase in pressure prior to the explosion, with three possible origins: magmatic push, important degassing and evaporation linked to magma/water interaction.

Because of the confinement, the last hypothesis seems unlikely in the South Sarigan case (Searcy, 2013). The resonance of a magma-gas mixture within either of a magmatic large chamber or conduit relatively near the surface of this submarine volcanic edifice (Dziak and Fox, 2002) seems more pertinent. If a gas-bearing cavity is compressed by slowly-rising magma, such a tremor-generating process would continue until magma ascent stops, interrupting the tremor but provoking then a strong increase of the constraints in the roof rocks, causing their break and the paroxysmal explosion. In agreement with the chronology and characteristics of the three tremors which immediately preceded the explosion (Fig. 18), we propose the following scenario (time spans before explosion and UTC times expressed as *hh:mn:ss*)

- *00:08:27; 11:39:20*: Rather intense tremor (140 Pa) presenting a maximum of energy near 3 Hz with some small punctual explosions of wider spectra, thus clearly different from tremors directly generated by explosive magmatic expansion (Fig. 4b). It could either mark the onset of fissuring or be associated with the fluctuation in the gaseous flow necessary for the resonance of the submarine cavity.
- *00:04:06; 11:43:41*: Original tremor of gliding frequency indicative of the resonance with an increasing frequency linked to the volume change of the cavity during magma ascent.
- *00:01:15; 11:46:31*: Clearly different from the two former ones, this tremor very close to the final explosion could indicate a weakening of the cavity roof due to pressure increase.
- *00:00:00; 11:47:47*: Paroxysmal explosion, contained within the magma chamber until decompression due to the swelling of the roof of this chamber and its opening, leading to the ejection through the water column of gases and ashes into the ocean and the atmosphere.

The recorded *T* phase corresponds to the portion of energy propagating in the liquid medium, and resulting first from the direct coupling between the underwater volcanic building and the water column,

610 and also from the noise generated by the transit of the products of the explosion to the ocean surface.
611 Seismic and hydrophonic recordings do not dissociate these two modes of generation, but the direct
612 coupling between the underwater volcanic edifice and the water column was probably predominant, while
613 transit within the water column likely represented a side effect that cannot account for the very impulsive
614 beginning of the *T* phase and the high intensity of the hydrophonic recordings.
615 Moreover, in the near field stations SARN (12 km), ANA2 (28 km) and ANNE (29 km) records, the
616 explosion was immediately followed by a saturated signal about 300 s long. Moderately large at SAP2
617 (156 km), this signal could be due to the repositioning of ejected materials, landslides and other geological
618 readjustments following immediately the explosion.
619
620 Such a scenario accounts for the spectacular recorded seismic and hydroacoustic effects, the
621 observation of a 12 km high atmospheric plume, a strong intensity of the infrasounds, hearing of the
622 explosion 13 km away in Sarigan Island and the first tsunami triggered by the ejection of gases and
623 materials through the c. 200 m deep water column overlying the submarine volcanic structure.
624
625 The second tsunami that occurred more than 2 hours later could not result from the explosion.
626 Data related to this late event include only a very small superficial wave in close field. According to our
627 experience, collapses or external landslides on the sides of the volcano, given the involved volumes of
628 materials, would have generated measurable hydroacoustic effects (at least on the very sensitive and well
629 positioned networks of hydrophones of Wake: H11N and H11S) and seismic waves (*Pg*) in close field.
630 That was not the case, but a landslide occurring on the far side of the volcano (i.e. facing west) would
631 also be much harder to detect via hydroacoustic arrays at Wake. Therefore, we can envision intra-
632 caldera collapse events of the newly-formed and still weak caldera walls. Filling of the caldera by
633 successive landslides slowed down by the viscosity of the water might account for the periods (30 to 40
634 minutes) abnormally long for a tsunami of this importance, involving slow motion of a relatively large
635 volume of materials.
636
637 **4. Conclusions**
638
639 1. The analysis of the geophysical records of the May 29, 2010 paroxysmal event that ended the
640 South Sarigan seamount crisis (*Pg, P, T* phases and infrasounds) shows that the explosive nature of its
641 source in the volcanic basement is confirmed by the similarity of the *P* phases with those of underground
642 nuclear tests and the application of discriminating criteria Ms versus mb.
643 2. The explosive nature of the source in the water is also confirmed by the application of the
644 identification criteria for hydroacoustic sources and the *T* phases exceptionally impulsive and of short
645 durations.
646 3. The comparison with artificial explosions (conventional and nuclear tests) and the application of
647 the methods of evaluation of their released energy allows us to estimate a minimal released energy of 1 kt

(4.2 x 10^{12} J) for the seismic effects of the shock and c. 1 t of equivalent TNT (i.e. 4.2 x 10^{9} J) for the hydroacoustic effects of the explosive source in the water. Of course, these evaluations must be considered with caution given the different origins of the explosive processes.

. 4. The strong energy of the explosive source is also confirmed by the comparison of these plume and infrasounds with those of paroxysmal explosions of the subaerial volcanoes Augustine and Kasatochi.

5. Epicentre locations using *T* phases in an oceanic environment are more precise than those based exclusively on *P* phases or on *Pg*, *Pn* and *P* phases.

Beyond its obvious interest for documenting the geological evolution of poorly known submarine volcanic edifices, the South Sarigan event represents a rare example of strong natural explosion in the marine and solid medium, and the only one that can be studied with reference to nuclear explosions. Indeed, only two sea-free nuclear experiments were conducted (Wigwam of 30 kt in the northeast Pacific on 14/05/1955 and Swordfish, lower than 20 kt, 740 km west of San Diego on 11/05/1962) and there are few or no available recordings of these events. Strong undersea chemical explosions include only the ITRI experiment and the CHASE series ranging from 50 to 1,000 t of TNT but for which only poor quality graphic recordings are available (Talandier and Okal, 2004). The present study might thus improve our knowledge of the detection and identification of oceanic explosive sources.

Acknowledgements

We thank Emile A. Okal for numerous discussions, and Jean-Yves Royer for his critical reading of an early version of the manuscript, which was considerably focused and improved following the pertinent suggestions of two anonymous reviewers.

References

Aki, K., M. Bouchon and P. Reasenberg, 1974. Seismic source function for an underground nuclear explosion. Bull. Seismol. Soc. Am., 64, N1, 131-148.

Aki, K. and R. Y. Koyanagi, Deep volcanic tremor and magma ascent mechanism under Kilauea, Hawaii. J. Geophys. Res. 86, 7095-7109, 1981.

Anderson, M. O., W. W. Chadwick, M. D. Hannington, S. G. Merle, J. A. Resing, E. T. Baker, D. A. Butterfield, S. Walker, Nico Augustin, 2017. Geological interpretation of volcanism and segmentation of the Mariana backarc spreading center between 12.7°N and 18.3°N. Geochemistry, Geophysics, Geosystems, DOI 10.1002/2017GC006813

Arnoult, K. M., J. V. Olson, C. A. L. Szuberla, S. R. McNutt, M. A. Garcés, D. Fee, and M. A. H. Hedlin, 2010. Infrasound observations of the 2008 explosive eruptions of Okmok and Kasatochi volcanoes, Alaska. Journal of Geophysical Research, 115, D00L15, doi:10.1029/2010JD013987.

Bache, T. C., 1982. Estimating the yield on underground explosion. Bull. Seismol. Soc. Am., 72, N6, S121-S168.

Baker, E.T., Embley, R.W., Walker, S.L., Resing, J.A., Lupton, J.E., Nakamura, K., de Ronde, C.E.J., Massoth, G.J., 2008. Hydrothermal activity and volcano distribution along the Mariana arc. Journal of Geophysical Research, 113, B08S09, http://dw.doi.org/10.129/2007/JB005423.

Bloomer, S.H., R.J. Stern, and N.C. Smoot, 1989. Physical volcanology of the submarine Mariana and Volcano Arcs. Bulletin of Volcanology, 51: 210–224.

Bowers, D. and N. D. Selby, 2009. Forensic Seismology and the Comprehensive Nuclear-Test-Ban Treaty. Annu. Rev. Earth Planet. Sci., 37, 209–36.

693 Brown, S. K., H. S. Crosweller, R. S. J. Sparks, E. Cottrell, N. I. Deligne, N. O. Guerrero, L. Hobbs, K. Kiyosugi, S. C.
694 Loughlin, L. Siebert and S. Takarada (2014). Characterisation of the Quaternary eruption record: analysis
695 of the Large Magnitude Explosive Volcanic Eruptions (LaMEVE) database. J. Appl. Volcanol., 3:5.
696 Caplan-Auerbach, J., R. P. Dziak, J. Haxel, D. R. Bohnenstiehl, and C. Garcia, 2017. Explosive processes during the
697 2015 eruption of Axial Seamount, as recorded by seafloor hydrophones, Geochem. Geophys. Geosyst., 18,
698 doi:10.1002/2016GC006734.
699 Chadwick, W. W., K. V. Cashman, R. W. Embley, H. Matsumoto, R. P. Dziak, C. E. J. de Ronde, T.-K. Lau, N.
700 Deardorff, and S. G. Merle, 2008. Direct Video and Hydrophone Observations of Submarine Explosive
701 Eruptions at NW Rota-1 Volcano, Mariana Arc. Journal of Geophysical Research, 113, B08S10, 1-23.
702 Chadwick, W. W., Jr., I. C. Wright, U. Schwarz-Schampera, O. Hyvernaud, D. Reymond, and C. E. J. de Ronde, 2008.
703 Cyclic eruptions and sector collapses at Monowai submarine volcano, Kermadec arc: 1998–2007.
704 Geochemistry Geophysic Geosystem, 9, Q10014, doi:10.1029/2008GC002113.
705 Chadwick, W. W., Jr, R.P. Dziak, J.H. Haxel, R.W. Embley and H. Matsumoto, 2012. Submarine landslide triggered by
706 volcanic eruption recorded by in situ hydrophone. Geology, 40, 51-54. doi: 10.1130/G32495.1.
707 Chouet, B., 1981. Ground motion in the near field of a fluid-driven crack and its interpretation in the study of shallow
708 volcanic tremor. J. Geophys. Res., 86, 5985-6016.
709 Chouet B., 1988. Resonance of a Fluid-Driven Crack, Radiation Properties and Implications for the Source of Long-
710 Period Events and Harmonic Tremor. Journal of Geophysical Research, 93, B5, 4375-4400.
711 Chouet B., 1992. A seismic model for the source of long-period events and harmonic tremor. in Volcanic Seismology,
712 edited by P. Gasparini, R. Scarpa, and K. Aki, pp. 133–156, Springer-Verlag, New York.
713 Clauter, D.A., Blandford, R.R., 1998. Capability modeling of the proposed International Monitoring System 60-Station
714 Infrasonic Network. LAUR-98-56, Los Alamos National Laboratory Report, Los Alamos, NM.
715 Cole, R., 1948. Underwater explosions, New-York Dover Publications Inc.
716 Crosweller HS, Arora B, Brown SK, Cottrell E, Deligne NI, Guerrero NO, Hobbs L, Kiyosugi K, Loughlin SC, Lowndes
717 J, Nayembil M, Siebert L, Sparks RSJ, Takarada S, Venzke E., 2012. Global database on large magnitude
718 explosive volcanic eruptions (LaMEVE). J Appl Volcanol 1(4):1–13, 10.1186/2191-5040-1-4
719 Dziak, R. P., C. G. Fox, 2002. Evidence of harmonic tremor from a submarine volcano detected across the Pacific
720 Ocean basin. Journal of Geophysical Research, 107, B5, 2085, 10.1029/2001JB000177.
721 Dziak, R. P., M. Park, H. Matsumotoa, S. K. Byunb, 2005. Hydroacoustic records and a numerical model of the source
722 mechanism from the first historical eruption of Anatahan Volcano,Mariana Islands. Journal of Volcanology
723 and Geothermal Research, 146, 86–101.
724 Dziak, R. P., E. T. Baker, A. M. Shaw, D. R. Bohnenstiehl, W. W. Chadwick Jr., J. H. Haxel, H. Matsumoto, and S. L.
725 Walker, 2012. Flux measurements of explosive degassing using a yearlong hydroacoustic record at an
726 erupting submarine volcano. Geochemistry Geophysic Geosystem, 13, Q0AF07, doi:10.1029/2012004211.
727 Embley R. W., Baker E. T., D. A. Nutterfield, W. W. Chadwick JR, J. E. Lupton, J. A. Resing, C. E.J. De Ronde, K. I.
728 Nakamura, V. Tunnicliffe, J. F. Dower and S. G. Merle, 2007. Exploring the Submarine Ring of Fires;
729 Mariana Arc – Western Pacific. Special Issue on Ocean Exploration, Oceanography, V20, N4.
730 Embley R. W., Tamura, Y., Merle, S.G., Sato, T., Ishizuka, O., Chadwick, W.W. Jr., Wiens, D.A., Shore, P., Stern,
731 R.J., 2014. Eruption of South Sarigan Seamount, Northern Marianas Islands: Insights into hazards from
732 submarine volcanic eruptions. Oceanography, 27, 24-31. http://dx.doi.org/10.5670/oceanog.37.
733 Fee, D., A. Steffke, and M. Garces, 2010. Characterization of the 2008 Kasatochi and Okmok eruptions using remote
734 infrasound arrays. Journal of Geophysical Research, 115, D00L10, doi:10.1029/2009JD013621.
735 Fee, D., R. Waxler, J. Assink, Y. Gitterman, J. Given, J. Coyne, P. Mialle, M. Garces, D. Drob, D. Kleinert, R.
736 Hofsteter, P. Grenard, 2013. Overview of the 2009 and 2011 Sayarim Infrasound Calibration Experiments.
737 Journal of Geophysical Research Atmosphere, 118, 6122–6143, doi:10.1002/jgrd.50398.
738 Ford, S. R. and W. R. Walter, 2014. mb: Ms Screening Revisited for Large Events. Bull. Seismol. Soc. Am., Vol. 104,
739 No. 3, doi: 10.1785/0120130182
740 Green, D., L. Evers, D. Fee, R. Matoza, M. Snellen, D. Simons, 2011. The South Sarigan submarine volcanic
741 eruption, May 2010: an example of International Monitoring System waveform data synergy. Presented at:
742 Comprehensive Nuclear-Test-Ban Treaty: Science and Technology, 2011, Hofburg Palace, Vienna.
743 Green, D., L. Evers, D. Fee, R. Matoza, M. Snellen, P. Smets, D. Simons, Hydroacoustic, infrasonic and seismic
744 monitoring of the submarine eruptive activity and sub-subaerial plume generation at South Sarigan, May
745 2010, 2013. Journal of Volcanology and Geothermal Research, 257, 31-43.
746 Gudmundsson, A., 2014. Elastic energy release in great earthquakes and eruptions. Frontiers in Earth Science, 2, 10,
747 1-12, doi: 10.3389/feart.2014.00010.
748 Harben, P. H., Terri F. Hauk, 2010. Background acoustic noise models for the IMS hydroacoustic stations. Lawrence
749 Livermore National Laboratory. 2010 Monitoring Research Review: Ground-Based Nuclear Explosion
750 Monitoring Technologies. Award No. DE-AC52-07NA27344/LL09-IRP-NDD02.
751 Hedervari, P., 1963. On the energy and magnitude of volcanic eruptions. Bull. Volcanol. 25, 374-385. Doi: 10.
752 1007/BF02596568.
753 Herrin G., Theory of the pulsation of the gas bubble produced by an underwater explosion, 1941. Colombia University,
754 NDRC C-4, 20-010.

Hill, D. P., 1969. Crustal Structure of the Island of Hawaii from Seismic-refraction measurements. Bull. Seismol. Soc. Am., 59 (1), 101-1030.

Hotovec, A. J., S. G. Prejean, J. E. Vidale, J. Gomberg, 2013. Strongly gliding harmonic tremor during the 2009 eruption of Redoubt Volcano. Journal of Volcanology and Geothermal Research, 259, 89–99.

Jellinek, A. M., and D. Bercovici, 2011. Seismic tremors and magma wagging during explosive volcanism. Nature, 470, 522-525.

Lawrence, M. W., 2004. Acoustic Monitoring of the global ocean for the CTBT. Comprehensive Nuclear-Test-Ban Treaty Organisation, Vienna, Austria. Proceedings acoustic 2004. 3-5 November 2004, Gold Coast, Australia.

Le Pichon, A., J. Vergoz, E. Blanc, J. Guilbert, L. Ceranna, L. Evers, and N. Brachet, 2009. Assessing the performance of the International Monitoring System's infrasound network: Geographical coverage and temporal variabilities. Journal of Geophysical Research, 114, D 08112, doi:10.1029/2008JD010907.

Lesage, P., M. Mora, G. E. Alvarado, 2006. Complex behavior and source model of the tremor at Arenalvolcano, Costa Rica. Journal of Volcanology and Geothermal Research, 157, 49–59.

Liebermann, R. C. and P. W. Pomeroy, 1969. Relative excitation of surface waves by earthquakes and underground explosions. Journal of Geophysical Research, 74, 1575-1590.

Marshall, P. D. and P. W. Basham, 1972. Discrimination between earthquakes and underground explosions employing an improved Ms scale. Geophysical Journal, 28, 431-458.

Marshall, P. D., D. L. Springer and H. C. Rodean, 1979. Magnitude corrections for attenuation in the upper Mantle. Geophysical Journal of the Royal Astronomy Society, 609-638.

Mason, B. G., Pyle, D. M., and Oppenheimer, C., 2004. The size and frequency of the largest explosive eruptions on Earth. Bull. Volcanol., 66, 735–748. doi: 10.1007/s00445-004-0355-9

Murphy, J. R. and R. A. Mueller, 1971. Seismic characteristics of underground nuclear detonations. Bulletin of the Seismological Society of America, 61, N6, 1693-1704.

Murphy, J. R. and B. W. Baker, 2001. Application of Network-averaged P-wave Spectra. Pure and Applied Geophysics, 158, 2123-2171.

Newhall, C. G., and Self, S., 1982. The volcanic explosivity index (VEI)—an estimate of explosive magnitude for historical volcanism. J. Geophys. Res. 87, 1231–1238. doi: 10.1029/JC087iC02p01231

Newman, A.V., and E.A. Okal, 1998. Teleseismic estimates of radiated seismic energy: The E/M_0 discriminant for tsunami earthquakes, Journal of Geophysical Research, 103, 26885-26898.

Okal, E. A., P. J. Alasset, O. Hyvernaud and F. Schindelé, 2003. The deficient *T* waves of tsunami earthquakes. Geophys. J. Int., 152, 416-432.

Paris, R., A. D. Switzer, M. Belousova, A. Belousov, B. Ontowirjo, P. L. Whelley, M. Ulvrova, 2012. Volcanic tsunami: a review of source mechanisms, past events and hazards in Southeast Asia (Indonesia, Philippines, Papua New Guinea). Nat. Hazards, Doi: 10.1007/s11069-013-0822-8.

Powell, T. W., J. Neuberg, 2003. Time dependent features in tremor spectra. Journal of Volcanology and Geothermal Research, 128, 177–185.

Prejean, S.G. and E. E. Brodsky, 2011. Volcanic plume height measured by seismic waves based on a mechanical model. Journal of Geophysical Research, 116, 1–13.

Pyle, D.M., 1995. Mass and energy budgets of explosive volcanic eruptions. *Geophys. Res. Lett.* 22, 563–566. doi:10.1029/95GL00052

Reymond, D., O. Hyvernaud, J. Talandier and E. A. Okal, 2003. T-wave detection of two underwater explosions of Hawaii on April 13, 2000. Bulletin of the Seismological Society of America, 93, 804-816.

Rougier, J., R. Stephen, J. Sparks, K. V.Cashman, S. K.Brown, 2018. The global magnitude–frequency relationship for large explosive volcanic eruptions. Earth and Planetary Science Letters 482, 621–629.

Rubin, K.H., Soule, S.A., Chadwick Jr, W.W., Fornari, D.J., Clague, D.A., Embley, R.W., Baker, E.T., Perfit, M.R., Caress, D.W., Dziak, R.P., 2012. Volcanic eruptions in the deep sea. Oceanography, 25, 142-157, http://dx.doi.org/10.5670/oceanog. 2012.12.

Searcy C., 2013. Seismicity Associated with the May 2010 Eruption of South Sarigan Seamount, Northern Mariana. Seismological Research Letters, V 84, N 6. 1055-1061.

Selby, N. D., P. D. Marshall, and D. Bowers, 2012. mb: Ms event screening revisited, Bull. Seismol. Soc. Am. 102, 88–97.

Smith,W. H. F., Sandwell, D.T., 1997. Global sea floor topography from satellite altimetry and ships depth soundings. Science, 277, 1956-1962.

Snellen, M., Evers, L., Simons, D.G., 2011. Modelling the long-range acoustic propagation for the May 2010 Sarigan volcano eruption. In Papadakis, J.S. (ed), Underwater Acoustic Measurements, Kluwer, Kos, Greece, 1361-1368.

Stern, R.J., Smoot, N.C., 1998. A bathymetric overview of the Mariana forearc. The Island Arc, 7, 525-540.

Talandier, J., E. A. Okal, 1984. The Volcanoseismic Swarms of 1981-1983 in the Tahiti-Mehetia Area, French Polynesia. J. Geophys. Res., 89, B13, 11,216-11,234.

Talandier, J., E. A. Okal, 1984. News surveys of Macdonald Seamount, South Central Pacific, following volcanoseismic activity, 1977-1983. Geophysical Research Letters, 1, N 9, 813-816.

Talandier, J., E. A. Okal, 1987. Seismic detection of underwater volcanism: The example of French Polynesia. Pure and Applied Geophysics, 125, 919–950.

Talandier, J., E.A. Okal, 1998. On the mechanism of conversion of seismic waves to and from T-phases in the vicinity of island shores. Bulletin of the Seismological Society of America, 88, 621-632.

Talandier, J., E.A. Okal, 2001. Identification Criteria for Sources of T-phases Recorded in French Polynesia. Pure and Applied Geophysics, 158, 567-603.

Talandier, J., O. Hyvernaud, E. A. Okal, P. F. Piserchia, 2002. Long-range detection of hydroacoustic signals from large iceberg in the Ross Sea, Antarctica. Earth and Planetary Science Letters, 203, 519-534.

Talandier, J., 2004. Seismicity of the Society and Austral Hotspots in the South Pacific: Seismic Detection, Monitoring and Interpretation of Underwater Volcanism. In "Oceanic Hotspots" Roger Hekinian, Peter Stoffers, Jean-Louis Cheminée Editors, SPRINGER.

Talandier, J., E. A. Okal, 2004. Hydroacoustic Signals from Presumed CHASE Explosions off Vancouver Island in 1969-1970: A modern Perspective. Geophysical Research Letters, 75, 2, 188-198.

Talandier J., and E. A. Okal, 2004. Amplitude-duration and other discriminants for seismically recorded hydroacoustic phases. EOS, Transactions America Geophysical Union, v. 85, No. 47, p. F1297, 2004 [abstract].

Talandier, J., O. Hyvernaud, D. Reymond and E. A. Okal, 2006. Hydroacoustic signals generated by parked and drifting icebergs in the Southern Indian and Pacific Oceans. Geophysical Journal International, 165, 817-834.

Talandier J., J. M. Guerin, O. Hyvernaud, 2011. Dissipated Energy by South-Sarigan paroxysmic Explosion and Discrimination on Hydroacoustic Wave forms. Presented at: Comprehensive Nuclear-Test-Ban Treaty: Science and Technology 2011, Hofburg Palace, Vienna.

Talandier J., O. Hyvernaud, D. Reymond, J. M. Guerin, H. Hebert, A. Le Pichon, 2011. Detection, Location and Screening of seismic, hydroacoustic, infrasound and tsunami waveforms associated with May 29, 2010 South Sarigan paroxysmic Explosion, Marianas islands. Presented at: Comprehensive Nuclear-Test-Ban Treaty: Science and Technology 2011, Hofburg Palace, Vienna.

Talandier J., O. Hyvernaud, E.A. Okal, 2013. New Advanced Discriminants for Explosive Hydroacoustic Phase, General Assembly of IASPEI Goteborg, Tisdag 2013.

Talandier J., E.A. Okal, 2016. A new source discriminant based on frequency dispersion for hydroacoustic phases recorded by *T-phase* stations. Geophysical Journal International, 206, 1784-1794.

Tepp, G., W. W. Chadwick, M. M. Haney, J. J. Lyons, R. P. Dziak, S. G. Merle, D. A. Butterfield, C. W. Young, 2019. Hydroacoustic, Seismic, and Bathymetric Observations of the 2014 Submarine Eruption at Ahyi Seamount, Mariana Arc. American Geophysical Union, doi: 10.1029/2019GC008311.

Vyacheslav, M.Z., C. Navarro, G. Reyes-Davila, J. Orozco, M. Breton, A. Tellez, G. Reyes-Alfaro and H. Vasquez, 2006. The methodology of quantification of volcanic explosions from broad-band seismic signals and its application to the 2004–2005 explosions at Volcan de Colima, Mexico. Geophys. J. Int., 167, 467-478, doi: 101111/j.1365-246X.2006.03108.x.

Watts, A. B., U. S. Ten Brink, 1989. Crustal structure flexure, and subsidence history of the Hawaiian Islands. J. Geophys. Res., 94, 10473-10500.

Waythomas, C. F., W. E. Scott, S. G. Prejean, D. J. Schneider, P. Izbekov, and C. J. Nye, 2010. The 7–8 August 2008 eruption of Kasatochi Volcano, central Aleutian Islands, Alaska, Journal of Geophysical Research, 115, B00B06, doi:10.1029/2010JB007437.

Weston, D. E., 1960. Underwater Explosions as Acoustic Sources. Proc. Phys. Soc. 76**,** 233.

Whitaker, R. W., 1995. Infrasonic monitoring, in Proceedings of the 17th Annual Seismic Research Symposium, Scottsdale, Arizona, pp. 997–1000, Phillips Laboratory, Hanscom AFB, Mass.

Wielandt, E., 1975. Generation of Seismic Waves by Underwater Explosions. Geophysical Journal of the Royal Astronomy Society, 40, 421-439.

Wright, C., William W. Chadwick Jr., Cornel E. J. de Ronde, Dominique Reymond, Olivier Hyvernaud, Hans-Hermann Gennerich, P. Stoffers, K. Mackay, M. A. Dunkin, and S. C. Bannister, 2008. Collapse and reconstruction of Monowai submarine volcano, Kermadec arc, 1998–2004. Journal of Geophysical Research, 113, B08S03, doi:10.1029/2007JB005138.

Yamamoto, T, T. Soya, S. Suto, K. Uto, A. Takada, K. Sakaguchi, K. Ono, 1991. The 1989 submarine eruption off eastern Izu peninsula, Japan: ejecta and eruption mechanisms. Bull. Volcanol., 53: 301-308.

Zimanowski, B., and R. Buttner, 2003. Phreatomagmatic explosions in subaqueous volcanism, in Explosive Subaqueous Volcanism J. D. L. White, J. L. Smellie, and D. A. Clague (Editors), American Geophysical Monograph 140, 51–60.